




Detecting Water Depth from Remotely Sensed Imagery Based on ELM and GA-ELM

Guizhou Zheng¹  · Weihua Hua¹ · Zhonghang Qiu² · Zimei Gong¹

Received: 24 February 2020 / Accepted: 12 November 2020 / Published online: 24 November 2020
© Indian Society of Remote Sensing 2020

Abstract

The shallow seawater depth inversion based on remote sensing technology is important for water depth detection, which is of considerable significance to marine engineering, shipping, and marine military security. In this study, we took the Taiping Island and its adjacent waters in the South China Sea as a test bed and developed a water depth inversion model on the basis of extreme learning machine (ELM) and extreme learning machine optimized by genetic algorithm (GA-ELM). In GA-ELM, the input weights and the hidden layer biases were optimized by genetic algorithm. The two models allowed the evaluation of nonlinear relationships between the reflectance of high-resolution imagery from WorldView-2 and actual water depth obtained from the S-57 sea chart. The eight bands of the high-resolution image and the actual water depth were used as the input layer and the output layer, and the sigmoid function was introduced as activation function. Finally, the model accuracy was evaluated by using mean relative error (MRE), root mean square error (RMSE), mean absolute error (MAE), coefficient of determination (R^2), and the regression analysis between the retrieved water depth and the actual data. The simulation results showed that the two models had better stability than the second-order polynomial regression, BP neural network, and RBF neural network. Furthermore, GA-ELM had a more compact network structure and better generalization ability than ELM. Thus, we concluded that GA-ELM had higher precision and could achieve a better inversion result in the experimental area.

Keywords Taiping Island · WorldView-2 · Water depth inversion · Extreme learning machine · Genetic algorithm

Introduction

Water depth is an important parameter of the marine environment, and its detection is of considerable significance for marine aquaculture, marine transportation, coastal science applications, marine engineering

construction, and marine military as well as shipping safety. Compared with traditional measurement methods such as shipborne sonar and airborne laser sounding, the water depth inversion method based on remote sensing has notable advantages in some aspects, such as short cycle, large monitoring coverage, high precision, and low cost, particularly in the territorial power dispute regions that the measurement vessel cannot reach. However, these models are not well applied in some special environments. In contrast, the nonlinear water depth inversion model based on multiband reflectivity has more advantages in data acquisition convenience, geographic and temporal extensiveness.

The theoretical interpretation model is relatively simple, but a lot of unknown parameters need to be addressed (Lyzena 1978; Lee et al. 1999; Eugenio et al. 2015; Kanno et al. 2011; Tian et al. 2007). So, its promotion and application are greatly restricted. The error of depth result caused by the transformation of seafloor reflectivity or

✉ Guizhou Zheng
zhenggz@cug.edu.cn

Weihua Hua
805517975@qq.com

Zhonghang Qiu
774701454@qq.com

Zimei Gong
3087347745@qq.com

¹ School of Geography and Information Engineering, China University of Geosciences, Wuhan, China

² School of Resource and Environmental Sciences, Wuhan University, Wuhan, China

water attenuation is an important difficulty of the model. The traditional model has poor portability and is not suitable to the complex environment in which the strong seawater absorption to light waves leads to the energy attenuation of light propagation and the weak echo signal of the substrate. We can evaluate the correlation between the actual water depth and the spectral reflectance by constructing a statistical model, but the internal optical parameters of the water body don't need to be addressed. So, the statistical models can meet this requirement well. Based on the known water depth points, the linear relationships between the relative value and the absolute value of water depth such as the ratio model are established (Lyzenga 1985; Van et al. 1991; Clark et al. 1987; Stumpf et al. 2003; Eugenio et al. 2015b). In the ratio method, there is no need to remove dark water. The method is convenient and stable because the number of empirical coefficients required is less. Compared with linear penalty, the ratio method has better depth penetration ability in relatively clear water area, but it still has some limitations, especially in the condition of increasing noise. However, the statistical model is simple but inefficient comparing with artificial neural networks. The main reason is that the modeling result of the statistical model on the unknown nonlinear function relation is not ideal. So, the water depth retrieved by the statistical model to retrieve water depth is not accurate enough. Compared with the traditional linear water depth inversion model, nonlinear models such as neural network and support vector machine can quickly establish the nonlinear relationship between the in situ depth measurement and the multispectral multiband reflectivity (Ceyhan and Yalçın 2010; Wang and Zhang. 2005; Heddami 2016; Zhu et al. 2013; Ghose et al. 2010; Zheng et al. 2017b; Huang et al. 2011).

However, a nonlinear water depth inversion method such as a neural network may face several issues, including difficult determination of the size and structure of neural network in advance, premature, weak generalization, overfitting, sticks to local optimum easily, low local search ability, and slow speed of convergence and learning. The methodology proposed in this study use the model of extreme learning machine (ELM) to estimate shallow seawater depth, which makes it has faster learning speed and better generalization performance than other traditional models. Due to the nonlinear structure of ELM, we can estimate the nonlinear relationship between water depth and reflectivity of multiband remote sensing image. The water depth inversion can be carried out without considering environmental factors related to optical remote sensing such as water turbidity, bottom material, and water phytoplankton. In order to dissolve the problem of local optimization, an optimized method was proposed by using genetic algorithms, in which the top structure and related

parameters (weights and thresholds) can be obtained simultaneously. The advantages of the model are fast training speed, low polymerization, and far away from the local optimum. Meanwhile, the requirements of spatial and repetitive depth measurement are also reduced. The simulation showed that the method was effective for water depth inversion.

Study Area and Dataset

The study area covered the Taiping Island and its adjacent waters, located in the northwest of the Zheng He Group Reef of the northern of the Nan Sha Islands. It lies between $10^{\circ}20'50''N$ and $10^{\circ}23'25''N$ latitude and between $114^{\circ}20'40''E$ and $114^{\circ}25'30''E$ longitude and has an approximate area of 56 km^2 (Fig. 1). The upper right quarter of the figure shows the WorldView-2 remote sensing image of the entire study area. The sampling points are plotted in the graph, where green points (280 datasets) represent the training dataset and red points (70 datasets) represent the test dataset. We selected a subarea of the study area as the experimental area, which is displayed in the red box of the figure. The TP Island is very important to navigation safety, shipwreck notification, meteorological monitoring, and international flight intelligence monitoring. Remote sensing is suitable for water depth inversion because the area near the island is far from the mainland, where there is a good ecosystem with clear seawater quality.

The data used in the study were a high-resolution image of the WorldView-2 satellite obtained on March 18, 2011, when the season was very dry, the sky was clear, and the clouds over the study area are relatively thin. The image covered the entire research area where the image quality was considerably good to identify the edges of the item. It contained eight multispectral bands with a spatial resolution of 1.8 m, such as the blue band (450–510 nm), green band (510–580 nm), red band (630–690 nm), near-infrared band (770–895 nm), and four additional bands such as the coast band (400–450 nm), yellow band (585–625 nm), red edge band (705–745 nm), and near-infrared band 2 (860–1040 nm), along with one panchromatic band with a spatial resolution of 0.5 m.

The band selection of bathymetric inversion is very important, in order to find out which bands are the most suitable input layer neurons for the network model, we explored the correlation coefficient of the reflectivity and the corresponding water depth at each band of the sampling point in the early stage. Correlation analysis shows that the absolute values of the correlation coefficient between reflectivity and water depth of each band are less than 0.5, and the distribution is relatively concentrated between

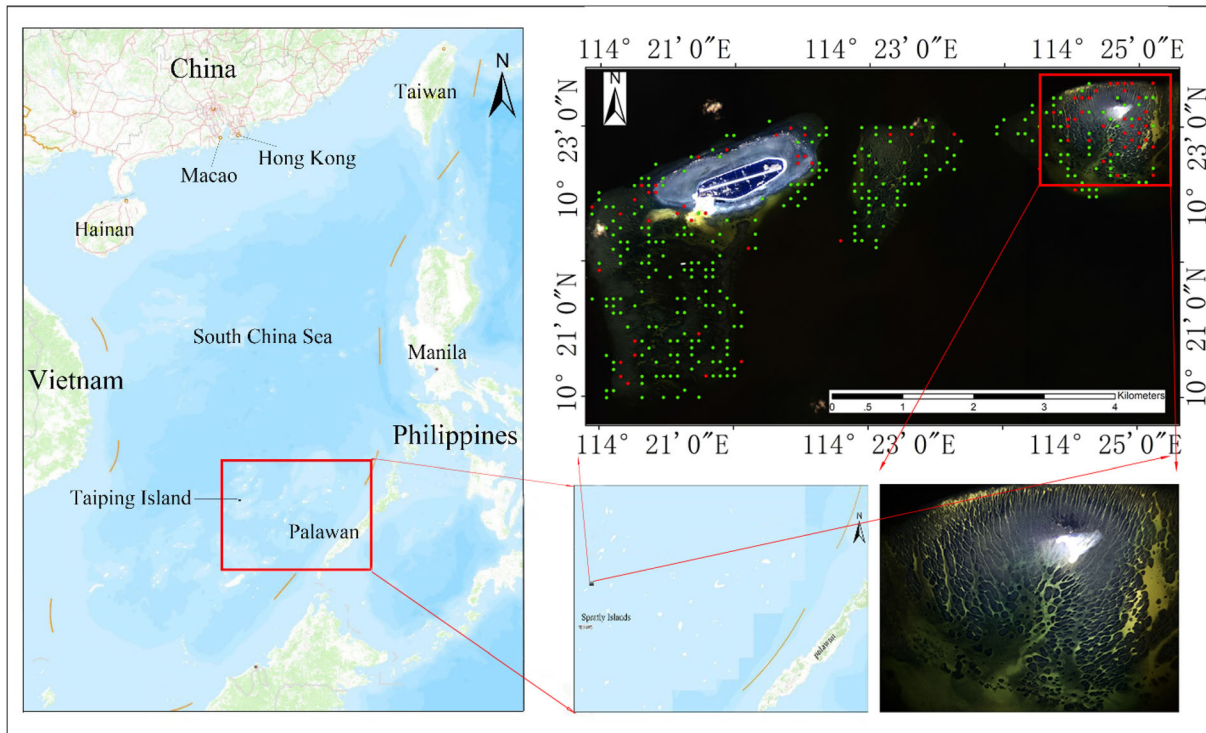


Fig. 1 Study area marked by the red box (color figure online)

0.3–0.5, only the values of correlation coefficient of coastal band and blue band are small. Therefore, it can be concluded that all the bands except the coastal band and the blue band can be used as the input layer of the model. However, both the coastal band and the blue band have the largest reflectance, the best penetrability and the least attenuation in water. Considering the correlation and spectral characteristics, all eight bands of worldview-2 remote sensing images were selected as the input layer. The actual water depth derived from the S-57 in the format of the electronic chart data of the same period was used as the output data of ELM, as shown in Fig. 2.

Methodology

ELM

Huang et al. proposed the extreme learning machine (ELM), which is a kind of machine learning algorithm designed for a feed forward neural network based on the traditional neural network (Huang et al. 2005, 2006). Compared with traditional neural network, it can improve learning efficiency and optimize parameter setting. Figure 3 shows the network structure of the model.

The single hidden layer feed forward neural network (SLFNs) is a kind of feed forward neural network with only

one hidden layer, which has been widely used due to its simple network structure and excellent function fitting ability. The ELM is a typical model of SLFNs, the feature mapping from input layer to hidden layer is given manually or randomly, and all it has to do is calculate the output weight. Therefore, it reduces the training time and the global optimal solution can be obtained easily. It consists of an input layer, a hidden layer, and an output layer. Here, it makes sense to connect each input layer neuron to each of the hidden layer neurons and each hidden layer neuron to each of the output layer neurons. For N arbitrary distinct samples (X_i, t_i) , where $X_i = [xi1, xi2, \dots, Xin]^T < Rn$, $t_i = [ti1, ti2, \dots, Tim]^T < Rm$. Assume that the hidden layer neuron is L ; then, N represents the input layer neuron, and M represents the output layer neuron. Therefore, the SLFNs with N hidden nodes and the activation function $g(x)$ can be described as follows:

$$\sum_{i=1}^L \beta_i g(W_i \cdot X_j + b_i) = o_j (i, j = 1, 2, \dots, N) \tag{1}$$

$$W_i = [w_{i1}, w_{i2}, \dots, w_{im}]^T$$

$$\beta_i = [\beta_{i1}, \beta_{i2}, \dots, \beta_{im}]^T$$

where X_j and o_j are the input and the output vectors, respectively; $g(x)$ is the hidden layer output function (activation function) of node i ; W_i represents the connection weights between the input layer and the i th node in the

Fig.2 Actual bathymetric contour extracted from S57 sea chart

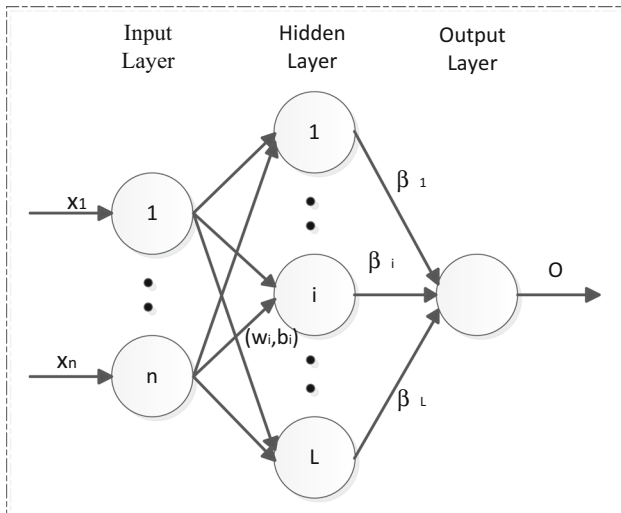
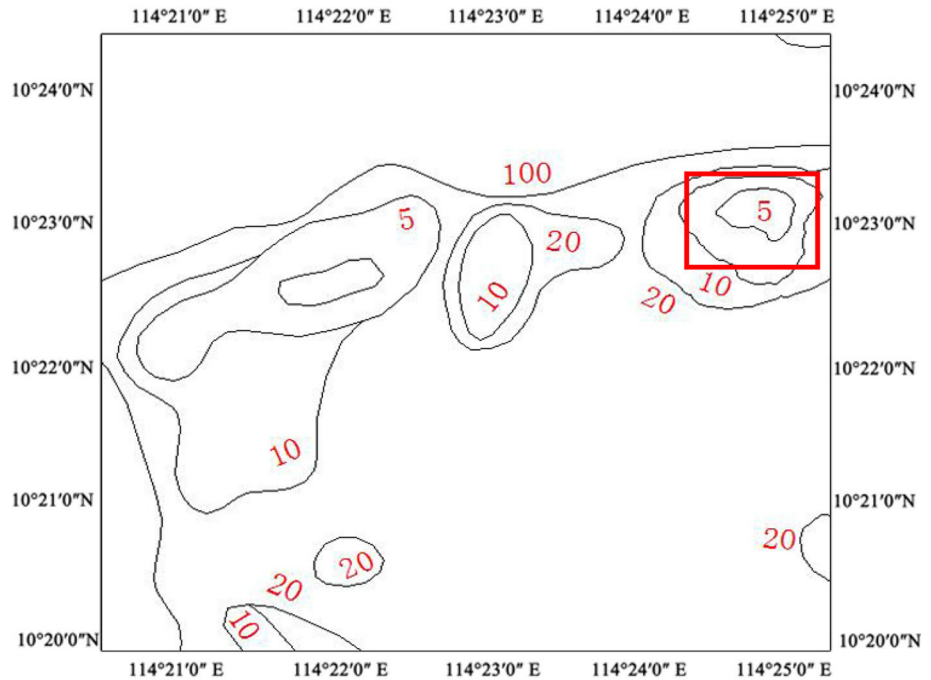


Fig.3 ELM network architecture

hidden layer; b_i is the bias of the i th hidden node; and β_i represents the connection weights between the i th node in the hidden layer and the output layer.

Activation function can help neural network model to understand and learn complex nonlinear relations. Due to the nonlinear relationship between band reflectivity and water depth, the activation function is introduced into the model to encode the nonlinear expression and capture the nonlinear factors of the data. Considering the characteristic of water depth inversion, we choose sigmoid activation function, which uses nonlinear method to normalize the

data and map all real numbers to (0, 1) interval. The sigmoid function is as follows:

$$g(x) = \frac{1}{1 + e^{-x}} \tag{2}$$

The standard SLFNs with L hidden nodes with the activation function $g(x)$ can approximate these N samples with zero error, implying that $\sum_{j=1}^L \|o_j - t_j\| = 0$. Further, there exist W_i , b_i , and β_i such that (Huang et al. 2006; Feng et al. 2009):

$$\sum_{i=1}^L \beta_i g(W_i \cdot X_j + b_i) = t_j(i, j, \dots, N) \tag{3}$$

Equation (3) can be written compactly as follows:

$$H\beta = T \tag{4}$$

where:

$$H = \begin{bmatrix} g(W_1 \cdot X_1 + b_1) & \dots & g(W_L \cdot X_1 + b_L) \\ \dots & \dots & \dots \\ g(W_1 \cdot X_N + b_1) & \dots & g(W_L \cdot X_N + b_L) \end{bmatrix}_{N \times L} \tag{5}$$

$$\beta = \begin{bmatrix} \beta_1^T \\ \beta_2^T \\ \dots \\ \beta_L^T \end{bmatrix}_{L \times M} \tag{6}$$

$$T = \begin{bmatrix} T_1^T \\ T_2^T \\ \dots \\ T_L^T \end{bmatrix}_{N \times M} \tag{7}$$

The complex matrix H is the hidden layer output matrix, β is the weight vector connecting the hidden neurons and the outputs, and T is the matrix of targets.

As rigorously proven in the theorems from Huang (Huang and Chen 2007, 2008; Huang et al. 2010), the input weights and the hidden layer biases can be randomly assigned if only the activation function is infinitely differentiable. W_i and b_i are not necessarily adjusted, and H can actually stay the same value once learning process starts. The objective of training a feed forward neural network is to minimize the training error and makes the predicted value more in line with the expected value. We can use the formula of $\min_{\beta} \|H\beta - T\|$ to find the optimal solution β of the equation $H\beta = T$.

$$\begin{aligned} \|H(W, B)\hat{\beta} - T\| &= \min_{\beta} \|H(W, B)\beta - T\| \\ W &= w_1, \dots, w_L \\ B &= b_1, \dots, b_L \end{aligned} \quad (8)$$

If the number L of the hidden nodes is equal to the number N of the distinct training samples, the matrix H is square and invertible when the input weight vectors W and the hidden biases b are randomly chosen, and SLFNs can approximate these training samples with zero error. However, in most cases, the number of hidden neurons is considerably less than the number of distinct training samples, and thus, we can obtain the optimal solution $\hat{\beta}$ of the equation $H\beta = T$ with the minimum output weights β :

$$\hat{\beta} = H^+T = (H^T H)^{-1} H^T T \quad (9)$$

where H^+ is the Moore–Penrose generalized inverse of the hidden layer output matrix H .

GA-ELM

The number of nodes in the hidden layer affects the accuracy of the ELM greatly. Due to the randomness of the input weight matrix and hidden layer bias initialized in the ELM, the partial 0 value will make the hidden node invalid and even reduce the precision of the model. Although the model accuracy can be improved by increasing the number of neurons, this may result in poor generalization (Han et al. 2013). Furthermore, even if it is same in the number of hidden layer neurons, the difference of input weight matrix and hidden layer bias will change the result of calculation and affect the stability and generalization performance of the inversion results. In this study, the parameters in the model were optimized by using the global search ability of genetic algorithm, during which they were adjusted by repeated training until met the accuracy requirement.

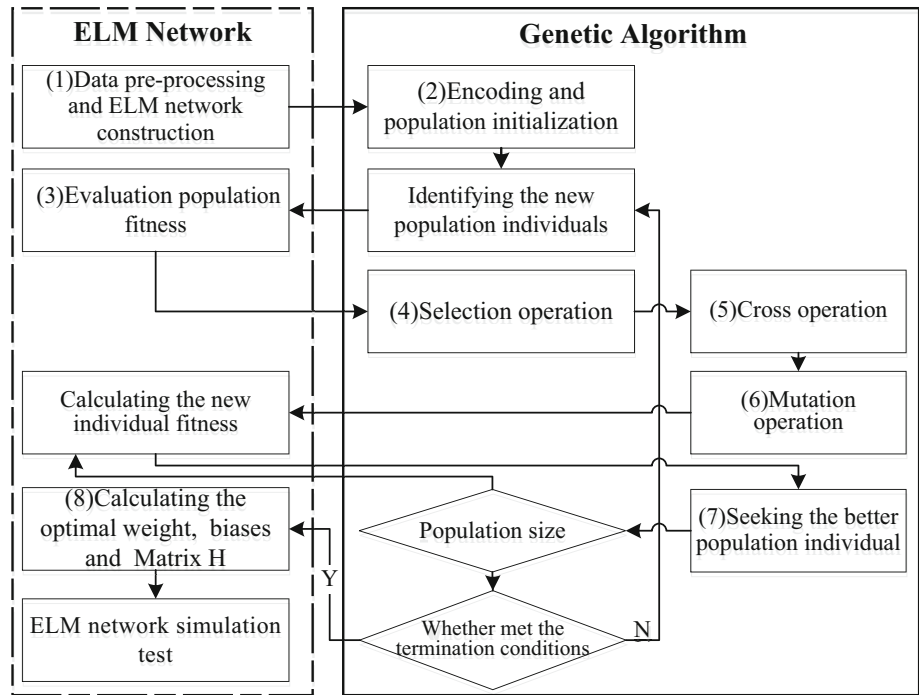
The input optimization of genetic algorithm is a global optimization method which simulates the natural selection and genetic mechanism of Darwin's biological evolution by referring to some features of biological evolution. Genetic algorithm adopts probabilistic optimization method, which can automatically acquire the optimized search space without definite rules and can adjust the search direction adaptively. Because the input weight matrix and hidden layer deviation of the extreme learning machine are given randomly, the hidden layer nodes will fail. Genetic algorithm performs well in global search ability and scalability. Therefore, the genetic algorithm was used to upgrade the model accuracy. The related workflow is shown in Fig. 4.

- (1) The ELM model has a fixed network structure, which is composed of the input neurons, the hidden neurons, and the output neurons. The training dataset and the test dataset constitute the data sample of the model.
- (2) The initial population of a group of input weights and hidden layer biases of ELM is usually randomly generated and can be of any desired size by the binary coding of the genetic algorithm.
- (3) Each member of the population is then evaluated by the “fitness” of the individual, which is calculated by how well it fits the desired requirements.
- (4) The overall fitness of the population is constantly improved by selection, which involves discarding the bad designs and only keeping the best individuals in the population.
- (5) New individuals are created by crossover, which combines various aspects of the selected individuals.
- (6) Mutation typically works by making very small changes at random to an individual's genome.
- (7) Once the next generation is generated, it automatically returns to step (3) until the optimal parameters are obtained and the network tends to converge.
- (8) The output matrix of hidden layer H is calculated according to the optimized weights and biases. The weights of the output layer are calculated based on the following equation: $\hat{\beta} = H^+T$. Finally, the simulation test is completed by using the trained network model.

Results

This study mainly includes the following two steps, establish the shallow seawater depth inversion model based on ELM and GA-ELM algorithm, and then evaluate the model accuracy on the basis of simulation training. The

Fig. 4 The network structure of ELM and GA-ELM



input layer of ELM or GA-ELM consisted of reflectivity of the WorldView-2 satellite image in eight multispectral bands, and the actual water depth obtained from S-57 in the format of electronic chart data as the output layer. In order to improve the inversion accuracy, the remote sensing images were preprocessed by means of geometric correction, atmospheric correction, and radiometric calibration. The predefined coordinate system in the study area is used to carry out the geometric correction. For each in situ position, which was evenly distributed in the region and was as similar as possible in each depth layers, the bands reflectivity of a single pixel was extracted from the corresponding image. In order to improve the efficiency of training, the input datasets were normalized as follows:

$$X = \frac{X_N - X_{MIN}}{X_{MAX} - X_{MIN}} \tag{10}$$

where X is the normalized data, X_N is the input data, and X_{MAX} and X_{MIN} are the maximum and minimum values of the input data, respectively.

Further, the output water depth of the network model was anti-normalized as follows:

$$X_N = X(X_{MAX} - X_{MIN}) + X_{MIN} \tag{11}$$

where X is the output water depth, X_N is the anti-normalized water depth, and X_{MAX} and X_{MIN} are the maximum and minimum values of the water depth, respectively.

In the training process, either too many or too few neurons will influence the training results. In order to analyze the influence of different numbers of hidden layer

neurons on the accuracy of the model, we used the RMSE as the evaluation index of the inversion results based on different neurons, gradually increased from 1 to 55 with the same model parameters. According to Fig. 5, we can conclude that fewer neurons do not produce desired result, the RMSE value decreased gradually with the increase in the number of hidden layer neurons, and the model obtained better generalization performance. Meanwhile, we observed that the neurons in ELM model tended to converge to 50 and that in GA-ELM model tended to converge to 20; moreover, GA-ELM exhibited a faster convergence speed than ELM.

The input layer weights and the hidden layer biases of the ordinary ELM network were randomly generated and left unchanged. The ELM model optimized by genetic algorithm can adjust the weight of the input layer and the

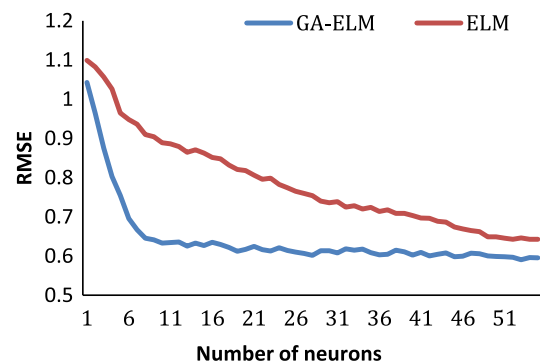


Fig. 5 Comparison of the RMSE values between ELM and GA-ELM with different number of neurons

bias of the hidden layer to get the optimal value. In order to control the evolutionary search for a satisfactory solution model, the genetic algorithm based on binary coding used five parameters (namely population size, generation gap, maximum evolution algebra, crossover rate, and mutation rate). The population size was 30, generation gap was 0.95, maximum evolution algebra was 100, crossover rate was 0.7 with the single-point crossover method, and the mutation rate was 0.01 with the binary mutation method. The iteration algorithm was used to obtain the optimal input layer weights and hidden layer biases, as shown in Fig. 6. As the evolution algebra increases, the training error gradually reduced and the evolution algebra of the GA-ELM network tended to converge to 44 in the iteration algorithm.

The actual water depth and the corresponding image data were selected as the sample datasets, and the simulation process was carried out in the MATLAB 6.5 environment. In all, 350 sets of sample data were used in this study. The scaled data of the reference points were divided randomly into the training dataset for the modeling and the testing dataset for the validation. Out of the 350 datasets, 280 datasets (training data) were selected to train randomly on the network, and 70 test datasets were used to evaluate the accuracy of the network model. The ratio of the training dataset to the test dataset was 4:1.

The value of mean relative error (MRE), root mean square error (RMSE), mean absolute error (MAE), and the coefficient of determination (R^2) was used to evaluate the model accuracy. A low MRE implied a small relative error; a low RMSE meant a small discrete degree; a low MAE value implied a narrow range of errors; and a high R^2 meant a good correlation between the in situ depth and the predicted value. Table 1 shows the inversion results, in which MRE is small, RMSE is smaller than 0.8, and MAE is less than 0.8 between the in situ depth and the predicted

value for ELM and GA-ELM. The performance comparison between the in situ depth measurement and the water depth inversion in the regression cases is given in the scatter diagrams that display the error and the deviation between them directly (Figs. 7 and 8). The sample point on the diagonal indicates that the depth of inversion is almost equal to the measured depth, and the sample point deviating from the diagonal indicates that the depth of inversion is quite different from the measured depth, in which case the better the fitting degree between the retrieved water depth and the measured water depth, the closer the retrieved water depth to the measured water depth. It can be seen that the values of R^2 (coefficient of determination) were all greater than 0.90 and reached 0.9258 and 0.9509, respectively. The water depth retrieved by the two methods is close to the measured water depth; however, the points in Fig. 8 are more compact and close to the fitting line than those in Fig. 7, which means GA-ELM method has better fitting effect on the verification set. Compared with ELM method, GA-ELM method has better fitting curve in the range of 7–12 m water depth and can achieve a better inversion result than the ordinary ELM. It can be seen from the table and the scatter diagrams that both ELM and GA-ELM achieved high inversion accuracy which indicates that the inversion results are reliable.

Figures 9 and 10 show the results of the two methods in the experimental area. It is obvious that the maximum water depth of the experimental area is approximately 12 m, the boundary between the sea and the island is clearly distinguished, the contour map based on GA-ELM is smoother than ELM, and the water depth is gradually increased from the island to the sea. A comparison with the S-57 sea chart data revealed that the water depth inversion results of the ELM and GA-ELM models were all consistent with the S-57 sea chart data in the experimental area; therefore, we concluded that the inversion results were reliable. Comparing the inversion results of the two models, it can be found that the inversion results based on ELM and GA-ELM are basically same in the 0–7 m water depth region, which shows that the inversion result of the water depth is better. In the 7–12 m water depth region, the inversion results of the two models are basically the same, but the edge is broken between the two adjacent water depth layers in Fig. 9, while the edge breakage is less obvious in Fig. 10; therefore, the inversion result based on GA-ELM is slightly better than the normal ELM, according to the analysis, it may be related to the optical attenuation in water body. The inversion results of the two models may differ in the details due to the accuracy.

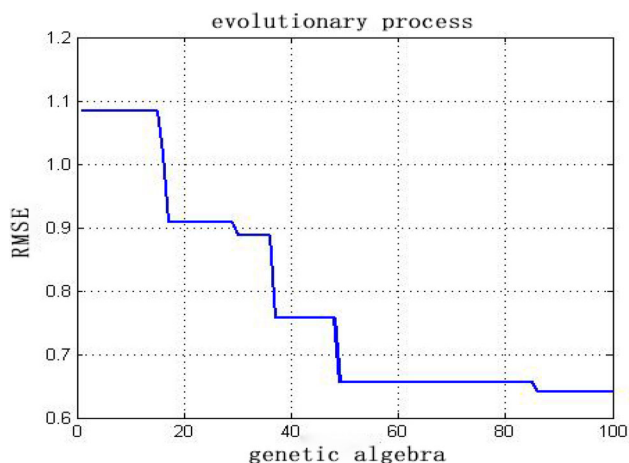
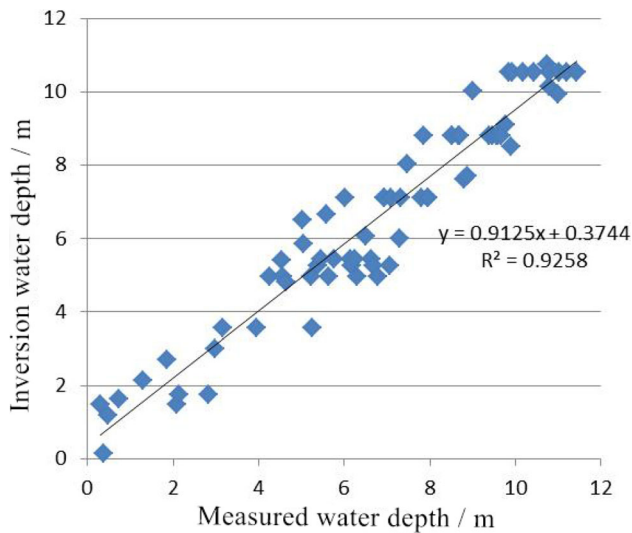
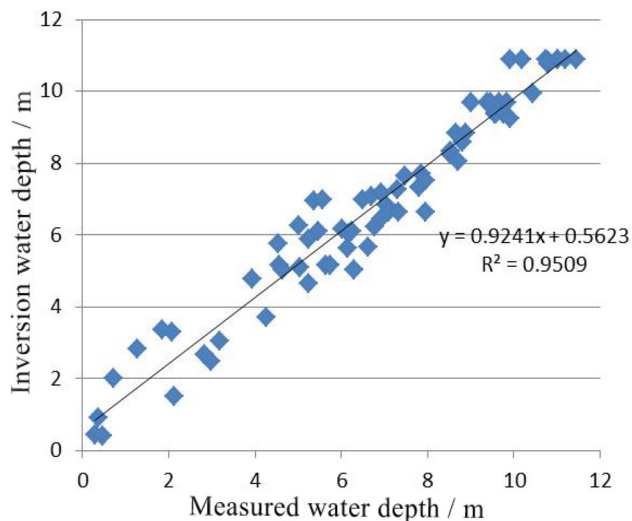


Fig. 6 Evolutionary iterative graph of genetic algorithms

Table 1 Accuracy evaluation form

Inversion model	MRE	RMSE	MAE	R^2	F	P value
ELM	22.05%	0.7734	0.7043	0.9258	0.1979	0.657
GA-ELM	11.51%	0.6288	0.5111	0.9509	0.0099	0.9208
Second-order polynomial regression	–	1.1616	–	0.8813	0.1174	0.8462
BP	–	1.8321	1.1493	0.9556	0.0008	0.9771
RBF	–	0.8922	0.4067	0.9959	0.0155	0.9011

**Fig. 7** Water depth inversion scatter plot of ELM**Fig. 8** Water depth inversion scatter plot of GA-ELM

Discussion

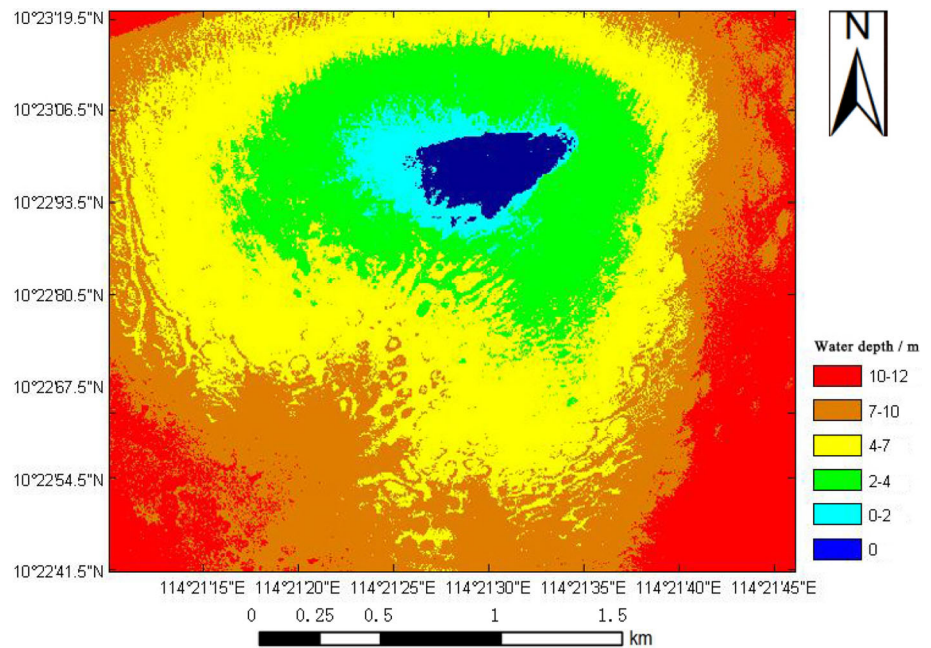
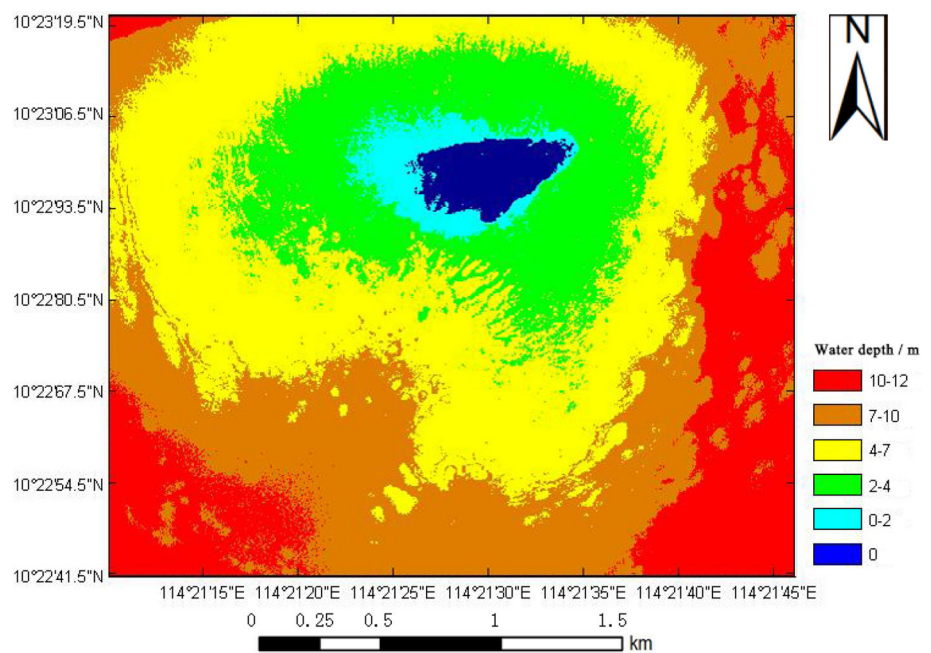
In addition to this study, we previously conducted shallow seawater inversion based on the second-order polynomial regression, a BP neural network, and an RBP neural network in the same region (Zheng et al. 2017a). Now, we

compare the results of this study with that of the previous three methods (Table 1).

GA-ELM and ELM (with R^2 of 0.9509 and 0.9258) exhibited an accuracy of 0.0696 and 0.0445 higher than the second-order polynomial regression model (with R^2 of 0.8813), but 0.0047 and 0.0298 lower than the BP model (with R^2 of 0.9556), and 0.045 and 0.0701 lower than the RBF model (with R^2 of 0.9959). Meanwhile, GA-ELM and ELM (with RMSE of 0.6288 and 0.7734) exhibited better stability than the second-order polynomial regression model (with RMSE of 1.1616), the BP neural network (with RMSE of 1.8321), and the RBF neural network (with RMSE of 0.8922). F value is less than F crit (3.9097), P value is more than 0.05, the results show that the inversion result is similar to the real water depth, and GA-ELM method has better stability than ELM algorithm.

The accuracy of the remote sensing water depth inversion was affected by many factors besides the inversion model, such as the marine environment, the S-57 electronic chart accuracy, and the quality of the remote sensing images. The specific influencing factors were as follows:

- (1) The preprocessing of high-resolution satellite images is a serious problem for the water depth inversion, because satellite images are susceptible to the natural variation of the sea level based on the normal wind waves and the tides based on the moon. However, the tide information cannot be obtained in the experimental area when the satellite transits. The water depth inversion may cause errors because there is no tide and wave correction.
- (2) The water depth inversion based on high-resolution satellite imagery is affected by the marine environment (particularly the water body substrate) and the difference in the optical properties of seawater. In order to improve the inversion precision, it is necessary to remove or reduce the influence of these environmental factors on the water depth inversion in the data preprocessing and data input.
- (3) The number of measured points on the S-57 electronic chart and the number of pixels on the image will affect the accuracy of the water depth inversion. They are too small to meet the accuracy requirements of the water depth inversion.

Fig. 9 Water depth inversion map of ELM**Fig. 10** Water depth inversion map of GA-ELM

- (4) The accuracy of the S-57 electronic chart depends on the water depth accuracy and the detection points distribution. The point distribution on the chart is too sparse and the water depth measurement values of individual areas on the map may be inaccurate, which inevitably affect the water depth inversion accuracy. In order to improve the accuracy, it is necessary that the water depth point be supplemented in the test area.
- (5) The seawater is taken as the satellite observation object, which is greatly affected by weather. For

example, under the condition of cloud and fog, the surface seawater is blocked by the clouds, and the reflection and radiation of the surface objects are blocked by the clouds. Therefore, satellite sensors cannot obtain effective spectrum information from the ground, which will greatly affect the results of water depth inversion. For the purpose of minimizing the influence of weather on inversion results, we use remote sensing image data at noon in dry season, during which time the sun shines directly into the

sky, the cloud layer and rain fall is less, and the image quality is higher.

Conclusions

In this study, we considered the Taiping Island and its adjacent waters in the South China Sea to be the research area. The traditional nonlinear water depth inversion model may face several issues such as complex network parameters, improper learning rate, and weak generalization ability. In this study, ELM and GA-ELM were used to invert the water depth based on the high-resolution WorldView-2 images and the S-57 sea chart data. From the performance comparison between ELM and GA-ELM, we concluded the following:

- (1) The shallow seawater depth of Nansha Islands in the South China Sea can be inverted by using the WorldView-2 satellite imagery, which is a more effective data support for studying the South Island reef, monitoring the sea environment, and ensuring the navigation security.
- (2) The GA-ELM can achieve better accuracy than ELM that can obtain good inversion results in the experimental area. The GA-ELM achieved a lower MRE value than ELM, down from 22.05% to 11.51%, a lower MAE value from 0.7043 to 0.5111, and a lower RMSE value from 0.7734 to 0.6288. We can conclude that the GA-ELM model had practical application value.
- (3) Although GA-ELM has a better network structure than the ordinary ELM, it takes a lot of time in the training process to get optimal parameters.

It is concluded in the study that the methodology proposed herein can be effectively provides an independent measure of the water depth at sample locations. Unlike the traditional linear water depth inversion model based on a single band or multiple bands, its nonlinear model free structure allows considering nonlinear relationships between reflectance from spectra different spectral bands of remote sensing image and water depths. The more accurate water depth could be estimated since ELM and GA-ELM models do not have to consider the factors affecting the reflective properties of water column sourced from environmental factors like bottom material and have few empirical coefficients required for the solution. The methodology can be practically applied without handling any complex reflectance separation process and subtracting dark water, and it can be reliably used for depth measurement provided that there is available representative input dataset. These results suggest that the model and

approach developed here can be used for making rapid surveys of water depth to reduce hazards to ship navigation, to construct marine engineering projects, to manage coastal zone, and to aid in investigation of ocean environment problems. Therefore, ELM and GA-ELM models have more advantages in data acquisition convenience, geographic and temporal extensiveness. Thus, the cost, labor, and time spend for detailed and repeated depth measurements could be significantly reduced.

Although the effectiveness of remote sensing technology in water depth inversion has been proved, it's worth noting that satellite imagery is more susceptible to environmental factors such as the atmosphere, tides, white water bubble, sun glint, wave, clouds, and fog than traditional methods (Strome and David 1990; Phinn et al. 2012). These factors increase the difficulty and error of determining water depth. We will focus on how to solve the impact of these factors on water depth inversion to improve its accuracy and reliability in the future.

References

- Ceyhun, Ö., & Yalçın, A. (2010). Remote sensing of water depths in shallow waters via artificial neural networks. *Estuarine, Coastal and Shelf Science.*, 89(1), 89–96.
- Clark, R. K., Fay, T. H., & Walker, C. L. (1987). A comparison of models for remotely sensed bathymetry (No. NORDA-145). NAVAL OCEAN RESEARCH AND DEVELOPMENT ACTIVITY STENNIS SPACE CENTER MS.
- Eugenio, F., Marcello, J., & Martin, J. (2015). High-resolution maps of bathymetry and benthic habitats in shallow-water environments using multispectral remote sensing imagery. *IEEE Transactions on Geoscience and Remote Sensing.*, 53(7), 3539–3549.
- Feng, G. R., Huang, G. B., Lin, Q. P., et al. (2009). Error Minimized Extreme Learning Machine With Growth of Hidden Nodes and Incremental Learning. *IEEE Transactions On Neural Networks*, 20(8), 1352–1357.
- Ghose, D. K., Panda, S. S., & Swain, P. C. (2010). Prediction of water table depth in western region, Orissa using BPNN and RBFN neural networks. *Journal of Hydrology.*, 394(3–4), 296–304.
- Han, F., Yao, H. F., & Ling, Q. H. (2013). An improved evolutionary extreme learning machine based on particle swarm optimization. *Neurocomputing*, 116, 87–93.
- Heddam, S. (2016). Secchi disk depth estimation from water quality parameters: artificial neural network versus multiple linear regression models. *Environmental Processes*, 3(2), 525–536.
- Huang, G. B., & Chen, L. (2007). Convex incremental extreme learning machine. *Neurocomputing*, 70(16–18), 3056–3062.
- Huang, G. B., & Chen, L. (2008). Enhanced random search based incremental extreme learning machine. *Neurocomputing*, 71(16), 3460–3468.
- Huang G B, Zhu Q Y, Siew C K. 2005. Extreme learning machine: a new learning scheme of feedforward neural networks// IEEE International Joint Conference on Neural Networks, 2004. Proceedings. IEEE, 2:985–990.
- Huang, G. B., Zhu, Q. Y., & Siew, C. K. (2006). *Extreme learning machine: Theory and applications Neurocomputing*, 70, 489–501.

- Huang, G. B., Ding, X. J., & Zhou, H. M. (2010). Optimization method based extreme learning machine for classification. *Neurocomputing*, 74(1–3), 155–163.
- Huang S, Jiang W G, Zhou T G, et al. 2011. Remote sensing of Extracting Water Depth based on Support Vector Machine. In: Proceedings of the 2011 International Conference on Future Computer Science and Application, Intelligent Information Technology Application Association, 381–384.
- Kanno, A., Koibuchi, Y., & Isobe, M. (2011). Statistical combination of spatial interpolation and multispectral remote sensing for shallow water bathymetry. *IEEE Geoscience and Remote Sensing Letters*, 8(1), 64–67.
- Lee, Z. P., Carder, K. L., Mobley, C. D., Steward, R. G., & Patch, J. S. (1999). Hyperspectral remote sensing for shallow waters 2 Deriving bottom depths and water properties by optimization. *Applied optics*, 38, 3831–3843.
- Lyzenga, D. R. (1978). Passive remote sensing techniques for mapping water depth and bottom features. *Applied Optics*, 17(3), 379.
- Lyzenga, D. R. (1985). Shallow-water bathymetry using combined lidar and passive multispectral scanner data. *International Journal of Remote Sensing*, 6(6), 115–125.
- Phinn, S. R., Roelfsema, C. M., & Mumby, P. J. (2012). Multi-scale, object-based image analysis for mapping geomorphic and ecological zones on coral reefs. *International Journal of Remote Sensing*, 33, 3768–3797.
- Strome WM, David E. 1990. Modern remote sensing digital image analysis technology for monitoring global change. In: Proceedings of the 23rd international symposium on remote sensing of environment, April 18, 1990-April 25.
- Stumpf, R. P., Holderied, K., & Sinclair, M. (2003). Determination of water depth with high-resolution satellite imagery over variable bottom types. *Limnology and Oceanography*, 48(1 part2), 547–556.
- Tian, Q. J., Wang, J. J., & Du, X. D. (2007). Study on water depth extraction from remote sensing imagery in Jiangsu coastal zone. *Journal of Remote Sensing*, 11(3), 373–379.
- Van Hengel, W., & Spitzer, D. (1991). Multi-temporal water depth mapping by means of Landsat TM. *International Journal of Remote Sensing*, 12(4), 703–712.
- Wang, Y. J., & Zhang, Y. (2005). Study on remote sensing of water depth based on BP artificial neural networks. *The Ocean Engineering*, 9(1), 26–35.
- Zheng, G. Z., Chen, F., & Shen, Y. L. (2017). Detecting the water depth of the South China sea reef area from WorldView-2 satellite imagery. *Earth Science Informatics*, 10, 331–337.
- Zheng, G. Z., & Le, X. D. (2017). Inversion of the water depth from WorldView-02 satellite imagery based on BP and RBF neural network. *Earth Science*, 42, 2345–2553.
- Zhu, Y., Zhao, Q., & Zhou, X. D. (2013). Remote sensing water depth inversion based on chaotic immune optimization RBF network. *Computer Engineering*, 39(5), 187–191.

Publisher's Note Springer Nature remains neutral with regard to jurisdictional claims in published maps and institutional affiliations.